frontiers | Frontiers in Energy Research RETRACTED ON 12 NOVEMBER 2025

TYPE Original Research
PUBLISHED 08 August 2024
DOI 10.3389/fenrg.2024.1442144

OPEN ACCESS

EDITED BY
Zening Li,
Taiyuan University of Technology, China

REVIEWED BY
Ruiyou Li,
Jiangxi University of Finance and Economics, China
Zhiping Zuo,
Chongqing University, China
Yushuai Li,
Aalborg University, Denmark

*CORRESPONDENCE
Jing Li,
xihuan_89@163.com

RECEIVED 01 June 2024
ACCEPTED 16 July 2024
PUBLISHED 08 August 2024
RETRACTED 12 November 2025

CITATION
Wang W, Cheng X, Li J, Zheng H and Li M (2024), Role of renewable energy and storage in low-carbon power systems.
Front. Energy Res. 12:1442144.
doi: 10.3389/fenrg.2024.1442144

RETRACTED: Role of renewable energy and storage in low-carbon power systems

Weiru Wang[1], Xueting Cheng[1], Jing Li[2]*, Huiping Zheng[1] and Mengzan Li[1]

[1]State Grid Shanxi Electric Power Research Institute, Shanxi Taiyuan, China, [2]China Electric Power Research Institute, Beijing, China

To promote the achievement of low-carbon goals in the power industry, rational and effective power system planning is essential. The participation of demand response in power system planning is an important means to reduce carbon emissions. To this end, a dual-layer low-carbon planning model for power systems considering carbon emission flow and demand response was designed. The upper layer investment planning model minimizes investment and operational costs, using an annual 8760-h operation simulation model and unit clustering linearization of the coal-fired units, coordinating the optimized investment and construction capacity of traditional units, new energy, and storage. The lower layer model forms a demand response model based on carbon emission flow theory and a load-side stepped carbon price mechanism, using the unit output and line flow data calculated by the upper layer model. This model reasonably adjusts the load distribution to reduce both the amount and cost of carbon emissions. Finally, the proposed model was analyzed and verified on the improved IEEERTS-24 node system.

KEYWORDS

low-carbon goals, power system planning, demand response, dual-layer planning model, carbon emission flow

1 Introduction

The extensive use of fossil fuels is depleting reserves and harming the global environment, necessitating an urgent shift to a low-carbon energy structure. To address the energy crisis and environmental degradation, it is urgent to transform the energy structure toward low carbonization. The proposal of the "carbon peak and carbon neutrality" goals provides clear guidance for promoting China's energy development along a low-carbon path (Salahi et al., 2020). Against the backdrop of low-carbonization energy, implementing a low-carbon planning of the power system, with clean energy as the main body, is an important approach to achieve the "dual carbon" targets. Effective carbon pricing mechanisms are central to this strategy, as they internalize the external costs of carbon emissions. Policymakers must establish robust carbon trading schemes to reflect these costs accurately, thereby incentivizing cleaner energy investments.

Even with high proportions of wind and photovoltaic (PV) power in future systems, coal-fired units persist, maintaining the carbon emission issues. The participation of demand response in the power system planning is crucial for reducing carbon emissions. Previous studies (Palmintier and Webster, 2016; Zhao et al., 2022; Zhang et al., 2023) primarily focused on the division of carbon emission responsibilities

between the generation and transmission sides, providing theoretical support but lacking practical guidance for user electricity usage and demand response in system planning. For instance, Palmintier and Webster (Zhao et al., 2022) discussed the impact of operational flexibility on generation planning but did not integrate demand response mechanisms (Asgharian and Abdelaziz, 2020; Guo et al., 2023; Li et al., 2024).

Demand response, as an important measure to ensure the safe, stable, and economic operation of the power system, has received wide attention from the academic and industrial communities (Mei et al., 2022). In power planning, the demand response adjusts the load on the user side, turning some rigid loads into adjustable flexible resources to participate in the operation of the power system, achieving adjustments and corrections to the load curve, thereby improving the efficiency of electricity use and reducing carbon emissions caused by unnecessary investments. In the research on demand response participation in grid planning, some studies have used data-driven methods to research and analyze the power system expansion planning and virtual power plant resource planning considering demand response, as well as power system coordinated planning schemes that include different types of user-side resources (Di Somma et al., 2015; Liang and Ma, 2022). Huang et al. (2021) studied a dual-layer coordinated planning model that combines short-term operational issues with long-term planning problems. However, the above methods did not consider the low-carbon benefits of demand response in power planning. Di Somma et al. (2015) constructed a grid planning model that combines demand-side management and low-carbon development; Chen et al. (2020) built a low-carbon transition planning model considering the demand response. Although the above literature verified that demand-side management can effectively reduce system carbon emissions, the responsibility for carbon emissions is still borne by the generation side.

The theory of carbon emission flows is an effective tool for analyzing carbon emission issues in the power system, promoting the development of low-carbon power technologies and providing important theoretical guidance for apportioning carbon emission responsibilities on the user side (Dimitriadis et al., 2023; Li et al., 2023). Many scholars have incorporated carbon emission flows into power planning. Some research designs for power planning are based on the carbon emission flow theory for site selection and capacity determination of power natural gas stations, as well as embedding the carbon emission flow model in the power grid expansion model. This model is used to allocate the overall carbon emission cap among regional multi-energy systems, coordinating planning at the regional level and across multiple regions (Cheng et al., 2019; Shen et al., 2020; Li et al., 2021). However, these studies have not involved the demand response aspects.

Although there are studies that propose low-carbon-oriented demand response operational planning models, which consider the low-carbon orientation of carbon emission flows on the user side demand, these models are inherently nonlinear. While they may be feasible for daily scheduling and planning issues, they are difficult to apply to the annual 8760-h power planning problems. This highlights the complexity of incorporating demand response and carbon emission flows into long-term planning models, indicating a need for further innovation and development in methodologies that can accommodate the nonlinearities and scale of such comprehensive planning efforts (An et al., 2017; Haghighi et al., 2021; Romero-Ávila and Omay, 2022).

Integrating the above discussions and analyses, this paper applies carbon emission theory to attribute the responsibility for carbon emissions in the power system to the user side. This approach aims to better leverage the role of demand-side response in promoting low-carbon transformation and to allocate carbon emission responsibilities more fairly and effectively. This approach reasonably apportions the carbon emission responsibilities among various load nodes. Combined with the demand-side stepped carbon price, using the carbon price as a price signal, this paper proposes an annual 8760-h power system dual-layer linear programming model that considers the apportionment of carbon emission responsibilities and active demand-side response. The upper layer planning is the traditional investment decision-making planning, mainly optimizing the capacity of traditional units, wind farms, PV stations, and energy storage devices in the system. Based on the upper layer planning, the lower layer planning utilizes the calculated power flows and the outputs of units and wind and solar power. It calculates the carbon emission responsibilities based on carbon emission theory, combined with the demand-side carbon price. Aiming to minimize the sum of carbon emission costs and demand response costs, it optimizes the load curve to achieve the goal of reducing both carbon emission volumes and costs.

2 Power system carbon emission flow

2.1 Overall logic of the low-carbon planning model

The low-carbon planning model proposed in this paper is a dual-layer approach that optimizes the installed capacity of power sources and energy storage, as well as user demand, through carbon emission flows and demand response. The upper layer is an investment planning model that determines the capacities of traditional units, wind farms, PV stations, and storage devices, along with their sequential outputs and transmission line flows. These outputs feed into the lower layer that first calculates node carbon potential and branch carbon flow density and then optimizes and adjusts the load curve to the output load adjustment power. The adjusted load data are subsequently fed back into the upper layer to update the investment planning.

Due to the large number of variables designed in the article, they are explained in Table 1. This facilitates the understanding of the variables involved in the formula.

2.2 Basic concepts

The concept of carbon emission flow (Kang et al., 2015; Wan et al., 2023) in power systems is defined as a virtual network flow attached to the power flow in the power system. It represents the carbon emissions generated to maintain the power network flow, essentially adding a carbon emission tag to the branch flows in the

TABLE 1 Definition of variables in the formula. Comparison of cost and total carbon emissions before and after demand response.

C_{Total}	Comprehensive system costs	$\theta_{i,t}$	Phase angle of node i
C_{Inv}	System investment cost	$a_{G,g}^{RD}$, $a_{G,g}^{RU}$	Maximum rate of downhill and uphill climb for conventional units
C_{Ope}	System operation cost	$P_{C,c,t}$	Output of unit group c at time t
N_G, N_{WT}, N_{PV} N_{ES}	Total number of conventional units, wind farms, photovoltaic plants, and energy storage devices	$Q_{c,t}$	Online start-up capacity of unit group c at moment t
$c_{G,g}^{Cap}$, $c_{WT,w}^{Cap}$, $c_{PV,p}^{Cap}$, $c_{ES,e}^{Cap}$	Investment costs per unit capacity for conventional units, wind farms, photovoltaic plants, and energy storage devices	$Q_{c,t}^{SD}$	Shutdown capacity of unit group c at time t
$Q_{G,g}$, $Q_{WT,w}$, $Q_{PV,p}$, $Q_{ES,e}$	Installed capacity of conventional units, wind farms, photovoltaic plants, and energy storage devices	$\lambda_{C,c}^{\min}$	Minimum output level of unit group c
N_T	Total number of time slots	$a_{C,c}^{RD}$, $a_{C,c}^{RU}$	Maximum rate of downclimb and upclimb for unit group c
N_c	Total number of crew groups	$T_{G,g}^{On}$, $T_{G,g}^{Off}$	Minimum start-up and shutdown times for conventional units
$c_{C,c}^{SU}$	Unit start-up cost of the unit group c	$\gamma_{WT,w,t}$, $\gamma_{PV,p,t}$	Output prediction curves for wind farms and photovoltaic plants
$c_{G,g}^{Gen}$, $c_{WT,w}^{Gen}$, $c_{PV,p}^{Gen}$, $c_{ES,e}^{Gen}$	Unit generation costs for unit group, wind farm, photovoltaic plant, and energy storage device	$S_{e,t}$	Charge state of energy storage devices
$Q_{c,t}^{SU}$	Starting capacity of unit group c at time t	η_e^{Cha}, η_e^{Dis}	Charging and discharging efficiency of energy storage devices
$P_{G,g,t}$, $P_{WT,w,t}$ $P_{PV,p,t}$	Generation output of units, wind farms, and photovoltaic plants at moment t	H_e	Duration of energy storage
$P_{ES,e,t}^{Dis}$, $P_{ES,e,t}^{Cha}$	Charging and discharging power of energy storage devices at time t	$E_{i,t}$	Carbon emissions from node i at time t
$\Omega_{G,i}$, $\Omega_{WT,i}$, $\Omega_{G,i}$, $\Omega_{ES,t}$	A collection of conventional units, wind farms, photovoltaic plants, and energy storage devices at node i	$C_{CE,i,t}$	Cost of carbon emissions at node i at moment t
B_l	Electro-nerve of branch l	c_{DR}	Demand response unit cost
$\Omega_{i+}\Omega_{i-}$	Collection of branch circuits injecting tidal currents into node i and flowing tidal currents out of node i	$D_{i,t}^{Up}$, $D_{i,t}^{Dn}$	Load upward and downward power adjustments at node i at moment t
$F_{l,t}$	Current of branch l at time t	$I_{L,l,t}$	Carbon flow intensity of branch l at time t
$\theta_{Bgn,l,t}$, $\theta_{End,l,t}$	Phase angle of the first and last nodes of branch l at time t	$I_{G,g,t}$, $I_{WT,w,t}$, $I_{PV,p,t}$	Carbon intensity of conventional units, wind farms and photovoltaic plants
$F_l^{\max}$	Maximum transmission capacity of branch l		

Before and after response	System investment costs (billion yuan)	System operation cost (billion yuan)	System comprehensive cost (billion yuan)	Total carbon emission cost of the system (billion yuan)	Total carbon emissions of the system (tCO2)
Before	915.826	10.397	926.223	18.517	6558598.555
After	841.234	10.294	851.528	16.185	6279634.733

power network. This can be further understood as follows: in the power system, carbon dioxide flows out from the generation side, follows the power generation into the power network, moves along the flows in the network, and finally flows into the load side. On the surface, it appears that carbon dioxide is directly emitted into the air from the generation side, but in essence, it is consumed by users on the load side through the carbon emission flow.

2.3 Basic definitions and calculation methods

According to the calculation method of carbon emission flow, if the output of the generation side, the carbon emission intensity, and the flow distribution of the entire power grid are known, then the distribution of carbon emission flow in the entire power system can

be calculated. This includes the carbon potential of each node and the carbon flow density of each branch. With this information, it is possible to transfer the carbon emission responsibility from the generation side to the user side and reasonably and effectively allocate the carbon emission responsibilities to each load node.

3 Low-carbon planning model for power systems

3.1 Assumptions of the model

3.1.1 Renewable energy availability

The model assumes consistent and predictable availability of renewable energy sources, such as wind and solar power. This is based on historical data and forecasted trends.

3.1.2 Demand response reliability

It is assumed that demand response mechanisms will be reliably triggered and effective in reducing peak loads. The model presumes that a certain percentage of the load can be shifted or curtailed as needed.

3.1.3 Carbon pricing stability

The model operates under the assumption that the carbon pricing will remain stable or follow a predictable trend. This includes the expectation that carbon markets will provide consistent signals to influence investment decisions.

3.1.4 Technological advancements

The model assumes ongoing advancements in energy storage and renewable energy technologies, which will enhance their efficiency and reduce costs over time.

3.1.5 Regulatory environment

A supportive regulatory environment is presumed, with policies that facilitate the integration of renewable energy and the implementation of demand response programs.

3.2 Investment planning model

3.2.1 Objective function of investment planning model

The objective of the investment planning model is to minimize the comprehensive cost of the system, which includes investment cost and operating cost. Specifically, the goal is to:

$$\min C_{Total} = C_{Inv} + C_{Ope}, \tag{1}$$

where C_{Total}, C_{Inv}, and C_{Ope} are the comprehensive cost of the system and the system investment.

The system investment cost includes traditional units, wind farms, and PV power stations, and the investment cost of energy storage equipment is as follows:

$$C_{Inv} = \sum_{g=1}^{N_G} c_{G,g}^{Cap} Q_{G,g} + \sum_{w=1}^{N_{WT}} c_{WT,w}^{Cap} Q_{WT,w} + \sum_{p=1}^{N_{PV}} c_{PV,p}^{Cap} Q_{PV,p} + \sum_{e=1}^{N_{ES}} c_{ES,e}^{Cap} Q_{ES,e}, \tag{2}$$

where N_G, N_{WT}, N_{PV}, and N_{ES} are the total number of traditional units, wind farms, PV power stations, and energy storage equipment, respectively; $c_{G,g}^{Cap}$, $c_{WT,w}^{Cap}$, $c_{PV,p}^{Cap}$, $c_{ES,e}^{Cap}$, $Q_{G,g}$, $Q_{WT,w}$, $Q_{PV,p}$, and $Q_{ES,e}$ are the unit capacity investment cost and installed capacity of traditional unit g, wind farm w, PV power station p, and energy storage equipment e, respectively.

The system operation cost includes the start-up cost and operation cost of traditional units, the operation cost of wind farms and PV power stations, and the operation cost of energy storage equipment, as follows:

$$C_{Ope} = \sum_{t=1}^{N_T}\sum_{c=1}^{N_c} c_{C,c}^{SU} Q_{c,t}^{SU} + \sum_{t=1}^{N_T}\sum_{g=1}^{N_G} c_{G,g}^{Gen} P_{G,g,t} + \sum_{t=1}^{N_T}\sum_{w=1}^{N_{WT}} c_{WT,w}^{Gen} P_{WT,w,t} + \sum_{t=1}^{N_T}\sum_{p=1}^{N_{PV}} c_{PV,p}^{Gen} P_{PV,p,t} + \sum_{t=1}^{N_T}\sum_{e=1}^{N_{ES}} c_{ES,e}^{Gen}\left(P_{ES,e,t}^{Dis} + P_{ES,e,t}^{Cha}\right), \tag{3}$$

where N_T and N_c are the total number of time periods and the total number of units respectively. $c_{C,c}^{SU}$ is the unit start-up cost of unit group c. $c_{G,g}^{Gen}$, $c_{WT,w}^{Gen}$, $c_{PV,p}^{Gen}$, and $c_{ES,e}^{Gen}$ are the unit power generation costs of unit g, wind farm w, PV power station p, and energy storage equipment e, respectively. $Q_{c,t}^{SU}$ is the start-up capacity of unit group c at time t. $P_{G,g,t}$, $P_{WT,w,t}$, and $P_{PV,p,t}$ are the power output of unit g, wind farm w, and PV power station p at time t, respectively. $P_{ES,e,t}^{Dis}$ and $P_{ES,e,t}^{Cha}$ are the charging and discharging power of energy storage device e at time t, respectively.

As the power system investment planning model established in this paper is based on an annual 8760-h sequential model, if the traditional unit combination modeling method is still used, computational efficiency cannot be guaranteed. Therefore, this paper adopts the unit clustering linearization method proposed in the literature for modeling traditional units.

3.2.2 Constraints of the investment planning model

The objective of the investment planning model is to minimize the comprehensive cost of the system, which includes investment cost and operating cost. Specifically, the goal is to

3.2.2.1 First item; installed capacity constraint

$$Q_{G,g} \le Q_{G,g}^{\max}. \tag{4}$$

$$Q_{WT,w} \le Q_{WT,w.}^{\max} \tag{5}$$

$$Q_{PV,p} \le Q_{PV,p.}^{\max} \tag{6}$$

$$Q_{ES,e} \le Q_{ES,e}^{\max}. \tag{7}$$

where $Q_{G,g}^{\max}$, $Q_{WT,w}^{\max}$, $Q_{PV,p}^{\max}$, and $Q_{ES,e}^{\max}$ are, respectively, the upper limits of installed capacity of traditional unit g, wind farm w, photovoltaic power station p, and energy storage device e. Eqs 4, 7 are used to limit the installed capacity of traditional units, wind farms, photovoltaic power stations, and energy storage equipment.

3.2.2.2 Proportion of new energy generation constraint

$$\sum_{t=1}^{N_t}\left(\sum_{w=1}^{N_{WT}} P_{WT,w,t} + \sum_{p=1}^{N_{PV}} P_{PV,p,t}\right) \ge \rho_{New}\sum_{t=1}^{N_T}\sum_{i=1}^{N_N} D_{i,t}^{Fore}, \tag{8}$$

where N_N is the total number of network nodes; ρ_{New} is the proportion of new energy generation; $D_{i,t}^{Fore}$ is the load demand forecasting curve of node i at time t. Formula 8 indicates that the ratio of the total power generation of wind farms and PV power stations to the total system load demand is not less than ρ_{New}.

The proportional coefficient ρ_{New} in Formula 8 represents the threshold above which the power generated by renewable energy sources must exceed the predicted load demand. This coefficient is selected based on several factors.

(1) Historical Data Analysis: We analyzed historical data on renewable energy generation and load demand to identify trends and variability patterns.
(2) Forecasted Trends: Future projections of renewable energy capacity and technological advancements are considered.
(3) Policy and Regulatory Requirements: Current and anticipated policies promoting renewable energy usage and carbon reduction targets are taken into account.
(4) System reliability and Stability: The coefficient is adjusted to ensure system reliability and stability, preventing over-reliance on intermittent renewable sources.

Specifically, ρ_{New} is chosen to strike a balance between maximizing renewable energy utilization and maintaining grid stability. For example, if historical data show that renewable energy can reliably meet 40% of the load demand, a slightly conservative value like 35% may be chosen for ρ_{New} to account for potential variability and ensure a buffer for unforeseen fluctuations.

3.2.2.3 Grid constraint

$$\sum_{g\in\Omega_{G,i}} P_{G,g,t} + \sum_{w\in\Omega_{WT,i}} P_{WT,w,t} + \sum_{g\in\Omega_{G,i}} P_{PV,g,t} + \sum_{e\in\Omega_{ES,t}} \left(P_{ES,e,t}^{Dis} - P_{ES,e,t}^{Cha}\right) - \sum_{l\in\Omega_{i-}} F_{l,t} + \sum_{l\in\Omega_{i+}} F_{l,t} = D_{i,t}^{Fore} \tag{9}$$

$$F_{l,t} = B_l\left(\theta_{Bgn,l,t} - \theta_{End,l,t}\right). \tag{10}$$

$$-F_l^{\max} \le F_{l,t} \le F_l^{\max}. \tag{11}$$

$$-\pi \le \theta_{i,t} \le \pi. \tag{12}$$

where $\Omega_{G,i}$, $\Omega_{WT,i}$, $\Omega_{G,i}$, and $\Omega_{ES,t}$ are the collection of traditional units, wind farms, PV power stations, and energy storage equipment of node i, respectively. B_l is the susceptance of branch l; Ω_{i+} and Ω_{i-} are the set of branches that inject power flow into node i and flow out of node i, respectively; $F_{l,t}$, $\theta_{Bgn,l,t}$, and $\theta_{End,l,t}$. are the power flow of the branch l at time t and the phase angles of the head and end nodes, respectively. $F_l^{\max}$ is the maximum transmission capacity of the branch; $\theta_{i,t}$ is the phase angle of node i. Eq. 9 is the node power balance equation. Eq. 10 is the branch DC power flow equation. Eqs 11, 12 are the upper and lower limit constraints of branch power flow and node phase angle, respectively.

3.2.2.4 Conventional unit operation simulation constraint

$$0 \le P_{G,g,t} \le Q_{G,g}. \tag{13}$$

$$-a_{G,g}^{RD} Q_{G,g} \le P_{G,g,t} - P_{G,g,t-1} \le a_{G,g}^{RU} Q_{G,g}, \tag{14}$$

where $a_{G,g}^{RD}$ and $a_{G,g}^{RU}$ are the maximum downhill and uphill speed of the traditional unit g, respectively. Eqs 13, 14 are the output and climbing constraints of the unit, respectively.

$$\lambda_{C,c}^{\min} Q_{c,t} \le P_{C,c,t} \le O_{c,t}. \tag{15}$$

$$-a_{C,c}^{RD} O_{C,t} \le P_{C,c,t} - P_{C,c,t-1} \le a_{C,c}^{RU} Q_{c,t}. \tag{16}$$

$$O_{c,t} = O_{c,t-1} + Q_{c,t}^{SU} - Q_{c,t}^{SD}. \tag{17}$$

$$O_{c,t} \ge \sum_{\tau=1}^{T_{C,c}^{On}} Q_{c,t-\tau+1}^{SU}. \tag{18}$$

$$O_{c,t} \le Q_{C,c} - \sum_{\tau=1}^{T_{C,c}^{Off}} Q_{c,t-\tau+1}^{SD}, \tag{19}$$

where: $P_{C,c,t}$, $Q_{c,t}$, and $Q_{c,t}^{SD}$ are, respectively, the output, online startup capacity, and shutdown capacity of group c at time t; $\lambda_{C,c}^{\min}$ is the minimum output level of unit group c; $a_{C,c}^{RD}$ and $a_{C,c}^{RU}$ are the maximum downslope and upslope speeds of group c, respectively. $T_{C,c}^{On}$ and $T_{C,c}^{Off}$ are the shortest startup and shutdown time of group c, respectively. $Q_{C,c}$ is the installed capacity of unit group c. Eqs 15, 16 are the output and climbing constraints of the unit group, respectively. Eq. 17 is the coupling relationship between the online startup capacity, startup capacity, and shutdown capacity of the unit group. Eqs 18, 19 are the minimum startup and shutdown time constraints of the unit group, respectively.

The following constraints represent the coupling relationship between units and groups of units:

$$P_{C,c,t} = \sum_{g\in\Omega_{G,c}} P_{G,g,t}, \tag{20}$$

$$Q_{C,c} = \sum_{g\in\Omega_{G,c}} Q_{G,g}, \tag{21}$$

$$^{SU}_{C,c} = \frac{\sum_{g\in\Omega_{G,c}} c_{G,g}^{SU} Q_{G,g}^{\max}}{\sum_{g\in\Omega_{G,c}} Q_{G,g}^{\max}}, \tag{22}$$

$$\lambda_{C,c}^{\min} = \frac{\sum_{g\in\Omega_{G,c}} \lambda_{G,g}^{\min} Q_{G,g}^{\max}}{\sum_{g\in\Omega_{G,c}} Q_{G,g}^{\max}}, \tag{23}$$

$$^{RD}_{C,c} = \frac{\sum_{g\in\Omega_{G,c}} a_{G,g}^{RD} Q_{G,g}^{\max}}{\sum_{g\in\Omega_{G,c}} Q_{G,g}^{\max}}, \tag{24}$$

$$a_{C,c}^{RU} = \frac{\sum_{g\in\Omega_{G,c}} a_{G,g}^{RU} Q_{G,g}^{\max}}{\sum_{g\in\Omega_{G,c}} Q_{G,g}^{\max}}, \tag{25}$$

$$T_{C,c}^{On} = \frac{\sum_{g\in\Omega_{G,c}} T_{G,g}^{On} Q_{G,g}^{\max}}{\sum_{g\in\Omega_{G,c}} Q_{G,g}^{\max}}, \tag{26}$$

$$T_{C,c}^{Off} = \frac{\sum_{g\in\Omega_{G,c}} T_{G,g}^{Off} Q_{G,g}^{\max}}{\sum_{g\in\Omega_{G,c}} Q_{G,g}^{\max}}, \tag{27}$$

where $\Omega_{G,c}$ is the unit set of the unit group c; $c_{G,g}^{SU}$ is the start-up cost of traditional unit g; $\lambda_{G,g}^{\min}$ is the minimum output level of the traditional unit g; $T_{G,g}^{On}$ and $T_{G,g}^{Off}$ are the shortest startup and shutdown time of traditional unit g, respectively. Formulas 20, 27 describe the relationships between unit and group outputs, installed

capacities, start-up costs, minimum output levels, maximum downslope and upslope climbing rates, and minimum startup and downtime periods for both units and groups.

3.2.2.5 Renewable energy output constraint

$$0 \le P_{WT,w,t} \le \gamma_{WT,w,t} Q_{WT,w.} \tag{28}$$

$$0 \le P_{PV,p,t} \le \gamma_{PV,p,t} Q_{PV,p.} \tag{29}$$

where $\gamma_{WT,w,t}$ and $\gamma_{PV,p,t}$ are the standard output prediction curves of wind farm w and PV power station p, respectively. Equation 28, 29 are the output constraints of wind farms and photovoltaic power stations, respectively.

3.2.2.6 Energy storage operation constraint

$$0 \le P_{ES,e,t}^{Dis} \le Q_{ES,e.} \tag{30}$$

$$0 \le P_{ES,e,t}^{Cha} \le Q_{ES,e.} \tag{31}$$

$$S_{e,t} = S_{e,t-1} + \eta_e^{Cha} P_{ES,e,t}^{Cha} - \frac{P_{ES,e,t}^{Dis}}{\eta_e^{Dis}}. \tag{32}$$

$$0 \le S_{e,t} \le H_e Q_{ES,e.} \tag{33}$$

$$S_{e,0} = S_{e,N_T} = \lambda_{ES,e}^{Lni} H_e Q_{ES,e.} \tag{34}$$

where $S_{e,t}$ is the state of charge of energy storage device e at time t; η_e^{Cha} and η_e^{Dis} are the charging and discharging efficiency of energy storage device e, respectively. H_e indicates the energy storage duration of energy storage device e. $\lambda_{ES,e}^{Lni}$ indicates the initial energy storage level of energy storage device e. Formulas 30, 31 are the discharge and charging power constraints of the energy storage device, respectively. Eq. 32 is the energy conservation constraint of the energy storage device. Formula 33 is the power limit constraint of the energy storage device; Formula 34 indicates that the initial moment of the energy storage device is consistent with the state of charge at the last moment.

3.2.2.7 System reserve constraint

$$\sum_{c=1}^{N_c} O_{c,t} + (1 - r_{New}) \left(\sum_{w=1}^{N_{WT}} \gamma_{WT,w,t} Q_{WT,w} + \sum_{p=1}^{N_{PV}} \gamma_{PV,p,t} Q_{PV,p} \right) + \sum_{e=1}^{N_{ES}} Q_{ES,e} \ge (1 + r_{Load}) \sum_{i=1}^{N_N} D_{i,t}^{Fore}, \tag{35}$$

where r_{New} and r_{Load} are the reserve rates of new energy generation and load demand, respectively. Formula 35 can ensure that the online startup capacity of the unit meets the standby requirements of the system operation.

3.3 Figures, tables, and schemes

3.3.1 Objective function of demand response model

The objective function of the demand response model is the minimum sum of carbon emission cost and demand response cost on the load side, which is given as follows:

$$\min \sum_{t=1}^{N_T} \sum_{i=1}^{N_N} \left[C_{CE,i,t} + c_{DR} \left(D_{i,t}^{Up} + D_{i,t}^{Dn} \right) \right], \tag{36}$$

$$C_{CE,i,t} = \begin{cases} c_{CE,1} E_{i,t} & 0 \le E_{i,t} \le E_{Bnd,1} \\ c_{CE,1} E_{Bnd,1} + & \\ c_{CE,2} \left(E_{i,t} - E_{Bnd,1} \right) & E_{Bnd,1} \le E_{i,t} \le E_{Bnd,2} \\ c_{CE,1} E_{Bnd,1} + & \\ c_{CE,2} \left(E_{Bnd,2} - E_{Bnd,1} \right) + & \\ c_{CE,3} \left(E_{i,t} - E_{Bnd,2} \right) & E_{Bnd,2} \le E_{i,t} \le E_{Bnd,3}, \\ c_{CE,1} E_{Bnd,1} + & \\ c_{CE,2} \left(E_{Bnd,2} - E_{Bnd,1} \right) + & \\ c_{CE,3} \left(E_{Bnd,3} - E_{Bnd,2} \right) + & \\ c_{CE,4} \left(E_{i,t} - E_{Bnd,3} \right) & E_{i,t} \ge E_{Bnd,3} \end{cases} \tag{37}$$

where $C_{CE,i,t}$ is the carbon emission cost of node i at time t; c_{DR} is the demand response unit cost; $D_{i,t}^{Up}$ and $D_{i,t}^{Dn}$ are, respectively, the upregulated and downregulated power of node i at time t. $E_{i,t}$ is the carbon emission of node i at time t; $c_{CE,1}$, $c_{CE,2}$, $c_{CE,3}$, and $c_{CE,4}$ are the unit cost of carbon emission. $E_{Bnd,1}$, $E_{Bnd,2}$, and $E_{Bnd,3}$ are the boundary quantities of carbon emission price range. Eq. 37 is the calculation formula of carbon emission cost at the load side.

3.3.2 Demand response model constraints

The objective function of the demand response model is the minimum sum of carbon emission cost and demand response cost on the load side, which is as follows:

3.3.2.1 Load regulation constraint

$$\begin{cases} 0 \le D_{i,t}^{Up} \le 0.2 D_{i,t}^{Fore} \\ 0 \le D_{i,t}^{Dn} \le 0.2 D_{i,t}^{Fore} \\ D_{DR,i,t} = D_{i,t}^{Fore} + D_{i,t}^{Up} - D_{i,t}^{Dn} \end{cases}. \tag{38}$$

$$\sum_{t=1}^{N_T} D_{DR,i,t} = \sum_{t=1}^{N_T} D_{i,t}^{Fore}. \tag{39}$$

where $D_{DR,i,t}$ is the load demand after node i responds at time t. In this paper, the adjustable ratio of node load is 20%. The first and second lines of Eq. 38 are the adjustable proportional constraints of the node load, and the third behavior responds to the equation of the node load before and after. Formula 39 can ensure that the system load before and after the response remains unchanged throughout the planning period.

3.3.2.2 Carbon emission equation constraint

$$E_{i,t} = I_{N,i,t} D_{DR,i,t}, \tag{40}$$

$$I_{L,l,t} = I_{N,i,t}, l \in \Omega_{i-}, \tag{41}$$

$$I_{N,i,t} = \frac{\sum_{g \in \Omega_{G,i}} P_{G,g,t} I_{G,g,t} + \sum_{w \in \Omega_{WT,i}} P_{WT,w,t} I_{WT,w,t} + \sum_{p \in \Omega_{PV,i}} P_{PV,p,t} I_{PV,p,t} + \sum_{l \in \Omega_{i+}} F_{l,t} I_{L,l,t}}{\sum_{g \in \Omega_{G,i}} P_{G,g,t} + \sum_{w \in \Omega_{WT,i}} P_{WT,w,t} + \sum_{p \in \Omega_{PV,i}} P_{PV,p,t} + \sum_{l \in \Omega_{i+}} F_{l,t}}, \tag{42}$$

where $I_{N,i,t}$ is the carbon potential of node i at time t; $I_{L,l,t}$ is the carbon flow density of branch l at time t; $I_{G,g,t}$, $I_{WT,w,t}$, and $I_{PV,p,t}$ are the carbon emission intensity of traditional unit g, wind farm w, and PV power station p, respectively. Eq. 40 is the equation constraint of node carbon emission. Formula 41 indicates that the branch carbon flow density of the power flow from the node is equal to the carbon

potential of the node. Eq. 42 is the constraint of the nodal carbon potential equation.

While wind turbines and PV units have negligible emissions during operation, their lifecycle emissions (IWT and IPV) must be considered. These values are derived from a LCA, which includes

(1) Manufacturing: emissions from producing the raw materials and manufacturing the components of wind turbines and PV panels.
(2) Transportation: emissions associated with transporting the components to the installation site.
(3) Installation: emissions from the construction and installation processes.
(4) Maintenance: emissions from ongoing maintenance activities throughout the operational life of the units.
(5) Decommissioning and Recycling: emissions from dismantling the units and recycling or disposing of the materials.

To calculate IWT and IPV, we use standard LCA methodologies and data from established databases such as Ecoinvent. The LCA approach provides a comprehensive view of the carbon footprint of these renewable energy units, ensuring that all phases of their lifecycle are accounted for.

For example, the LCA for a wind turbine includes the energy and emissions involved in producing steel for the tower, the composite materials for the blades, and the electronics for the control systems. Similarly, the LCA for PV panels considers the energy used in silicon purification, cell production, module assembly, and installation. By summing these emissions and dividing by the total energy output over the lifetime of the unit, we obtain the emission intensity values IWT and IPV.

3.4 Solution process

In the dual-layer low-carbon planning model designed in this paper, the lower layer model adjusts the distribution of system load through demand response, necessitating the updated load data to be fed back into the upper layer model for re-solving to optimize the planning results. Therefore, the solution process of the dual-layer low-carbon planning model is as shown in Figure 1.

(1) Input the planning parameters required for model solving, such as line parameters, unit parameters, wind and solar forecast curves, load forecast curves, and carbon emission coefficients.
(2) Solve the upper layer investment planning model, output the unit output, wind and solar output, and branch flows, and pass these into the lower layer model.
(3) Solve the demand response model with carbon price as the price signal and optimize the load adjustment.
(4) Update the load data after the response back into the upper layer model, re-solve the investment planning model, output the optimal planning results at this time, and calculate the carbon emissions and carbon emission costs on the load side.

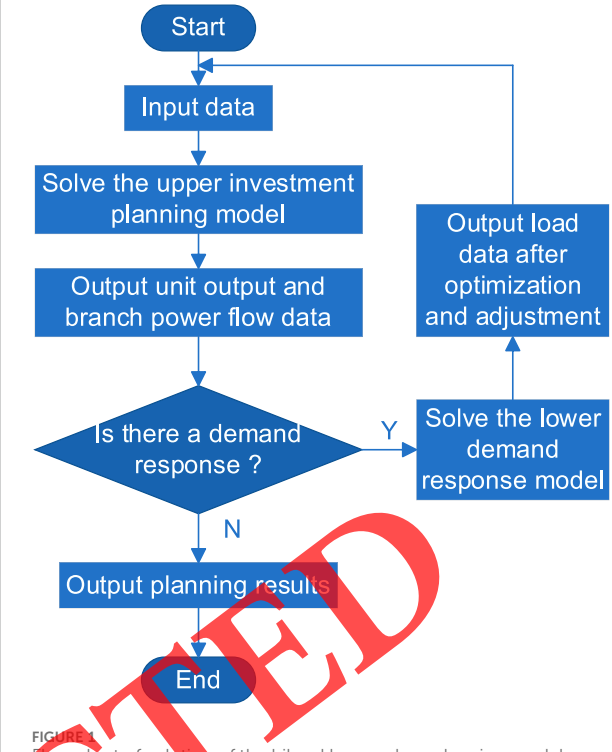

FIGURE 1
Flow chart of solution of the bilevel low-carbon planning model.

4 Low-carbon planning model for power systems

To analyze and validate the low-carbon planning method proposed in this paper, the IEEERTS-24 node system is used as an example. This system includes 24 nodes and 38 branches, representing a scalable model applicable to larger or smaller grids. By adjusting the input parameters, such as the number of nodes and branches, the model can be tailored to fit different grid sizes. For instance, in a smaller municipal grid, the model can focus on optimizing local renewable energy sources and storage solutions. Conversely, for a larger national grid, it can manage the integration of diverse energy resources across extensive geographical areas, ensuring efficient and reliable power delivery.

The IEEERTS-24 node system is modified to include traditional units, wind farms (WT), PV power stations, and energy storage devices. The traditional units have four types of installed capacity. Each renewable energy station is equipped with an energy storage device. Annual 8760-h wind and solar output curves and load demand curves are obtained using new energy-forecasting methods and load-forecasting methods.

The design logic for the carbon emission interval boundary and its carbon price is as follows: first, the carbon emission responsibilities on the load side are divided using the Shapley value-based carbon responsibility allocation method, determining the reasonable range of carbon emission responsibilities for each load node, i.e., the minimum and maximum values of carbon emission responsibility. Then, based on the carbon trading cost model, the incremental carbon emissions for each step are calculated, thus determining the carbon price interval boundary

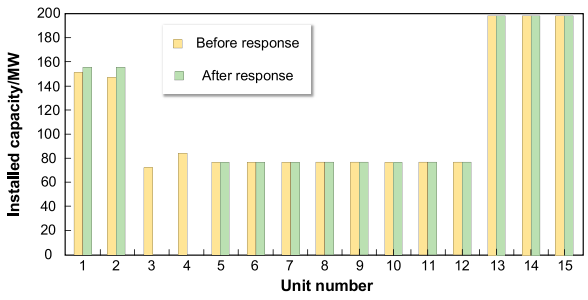

FIGURE 2
Comparison of optimization results of installed capacity of the traditional unit before and after demand.

for each node. The carbon prices for each interval are determined based on the average carbon price in China's domestic carbon market in 2020.

As the power system low-carbon planning model established in this paper is a linear programming problem, it is solved using the YALMIP optimization toolbox on the MATLAB platform, with the CPLEX solver called to solve the model.

4.1 Investment planning model

Based on the dual-layer low-carbon planning method proposed in this paper, the investment planning models before and after demand response are solved, and the comparative analysis of the planning results is shown in Figures 2, 3, and Table 1.

Figures 2, 3 show the comparison of the optimized installed capacities of traditional units, new energy, and energy storage devices before and after demand response. It can be analyzed from the figures that, compared to before demand response, the total installed capacities of traditional units, new energy, and energy storage devices have all decreased after demand response, with the reduction percentages being 8.65%, 2.71%, and 1.05%, respectively.

Table 1 presents a comparison of the system construction costs before and after demand response. As shown in Table 1, the investment cost, operating cost, and comprehensive cost of the system after demand response are all lower than before demand response, with reductions of 8.14%, 0.99%, and 8.06% respectively. This indicates that considering demand response in the low-carbon planning model can effectively reduce the construction costs of the system.

4.2 Analysis of carbon emission results

Based on the calculation results of the upper layer investment planning model, the carbon emission costs are calculated using carbon emission flow theory. The analysis of the system's carbon emissions before and after demand response is presented in Table 1. It is clear that the total annual carbon emissions and carbon emission costs of the system have decreased by 4.253% and 1.26%, respectively.

The analysis of the carbon emission results before and after demand response indicates that the low-carbon planning method proposed in this paper is effective in reducing the system's carbon emissions, leading to a reduction in carbon emission costs.

4.3 Analysis of sequential operation results

The analysis of the system's operational state during peak and off-peak days of system load is illustrated in Figures 4–6.

From Figure 4, it can be observed that after demand response, the overall system load demand is reduced, resulting in a significant decrease in the output of traditional units, while the output of new

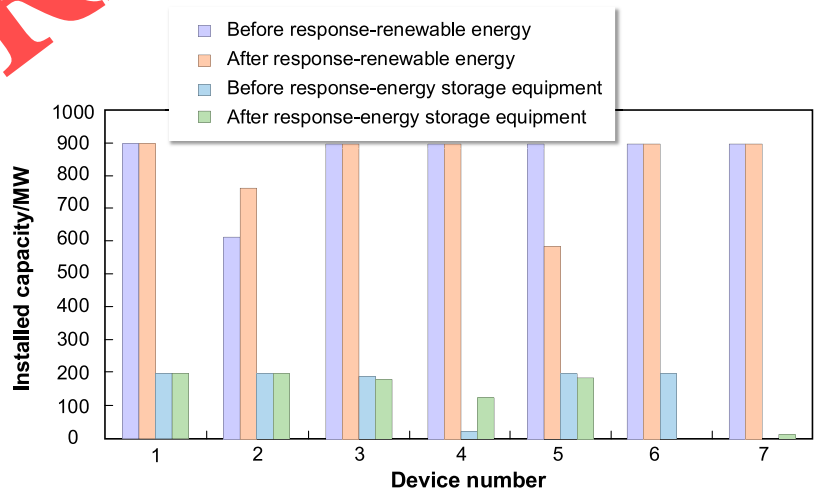

FIGURE 3
Comparison of optimization results of installed capacity of renewable energy and energy storage equipment before and after demand response.

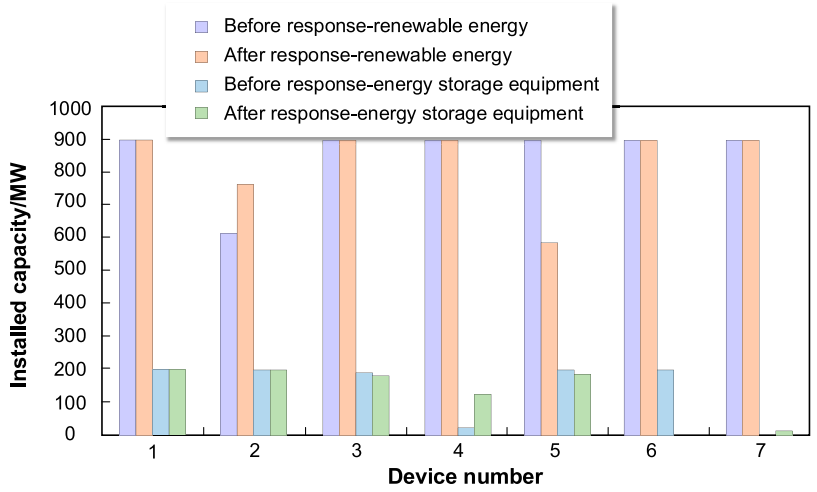

FIGURE 4
Curves of traditional unit output, renewable energy output, and load change before and after demand response on peak day.

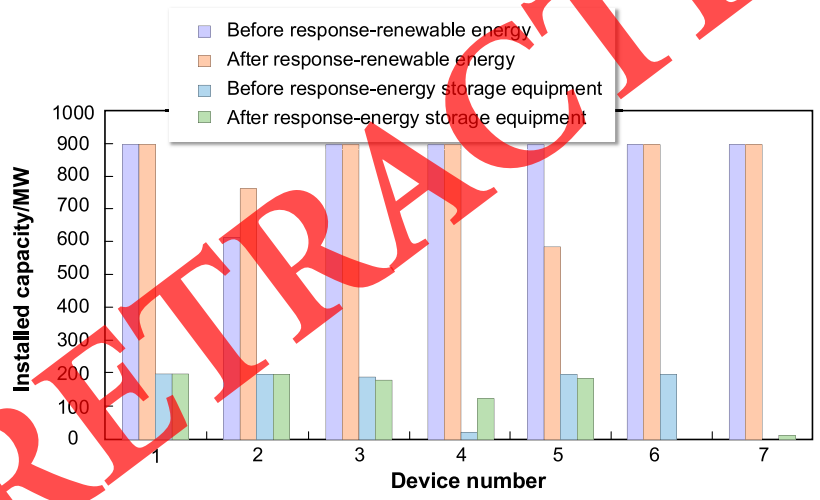

FIGURE 5
Curve of energy storage charging and discharging power change before and after demand response on load peak day.

energy sources is only slightly adjusted downward during the 9 to 20 time period. This suggests that to reduce the system's carbon emissions, it is crucial to minimize the output of traditional units while maintaining the output level of new energy sources. This reduction is further incentivized by effective carbon pricing mechanisms, which policymakers need to establish or enhance to reflect the true cost of carbon emissions. Furthermore, Figure 5 shows that energy storage is continuously charging during periods of high output from new energy sources, ensuring the absorption of new energy. In addition, due to the reduced system load, the charging power of the energy storage post-response is lower compared to pre-response. In periods 19 to 24, where new energy output is limited, the reduction in output from traditional units is less compared to other periods, and to meet the system load demand, energy storage begins to discharge. Similarly, due to the reduced system load, the post-response energy storage discharge power is also lowered.

Figure 6 indicates that in periods 1 to 7, with insufficient output from new energy, traditional units have to increase their output to meet load demand. Combined with Figure 7, it is evident that energy storage also needs to discharge, which leads to increased carbon emissions in the system. Therefore, post-response load demand is reduced. During periods 7 to 17, when new energy is abundant, load power is increased to promote the absorption of new energy, and energy storage is kept in a charging state. At the same time, to reduce carbon emissions, the output of traditional units drops sharply. In periods 17 to 24, with the output level of new energy insufficient, traditional units must increase output and energy storage must discharge to meet the load demand at that time. The extent of load increase gradually reduces, and the post-response output of

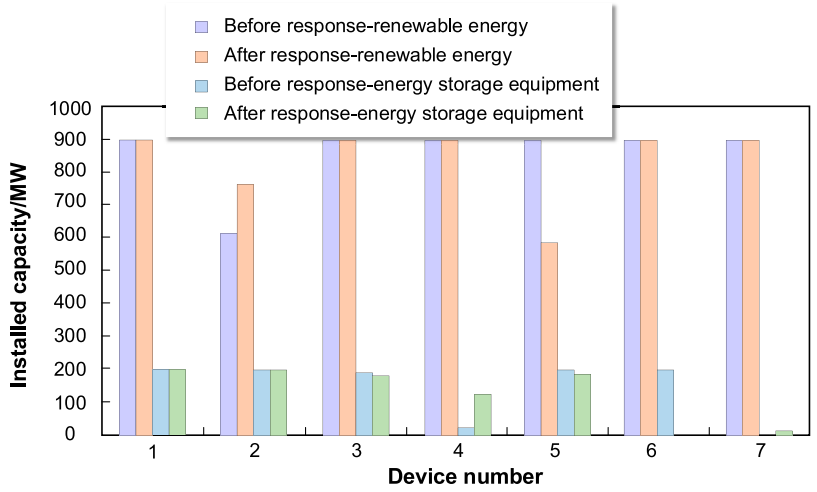

FIGURE 6
Curve of traditional unit output, renewable energy output, and load change before and after demand response on load valley day.

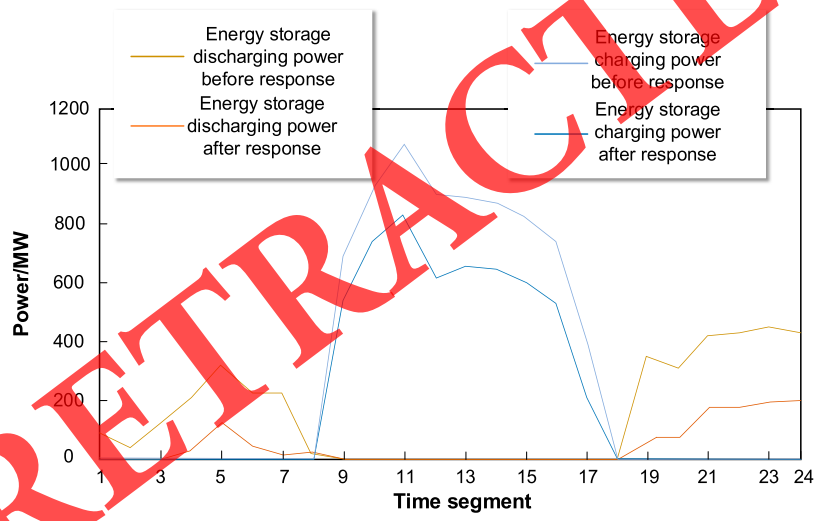

FIGURE 7
Curve of energy storage charging and discharging power change before and after demand response on load valley day.

traditional units is higher than pre-response because the post-response load has increased, and the post-response energy storage discharge power is also reduced.

4.4 Analysis of planning results for conventional demand response and low-carbon demand response

To verify the low-carbon guiding effect of carbon emission flow on demand response, a comparison was made between planning results that consider both carbon emission flow and demand response (low-carbon demand response) and those that only consider demand response (conventional demand response), as shown in Figures 8, 9.

From the analysis of Figures 8, 9, it can be seen that the installed capacities of traditional units are the same for both conventional and low-carbon demand response, at 1509 MW. This is the result of the demand response itself and is independent of whether carbon emission flow is considered or not. However, the total installed capacity of new energy is higher for low-carbon demand response than for conventional demand response, being 5851.57MW and 5753.3 MW, respectively. This indicates that low-carbon demand response requires an increase in new energy installed capacity and generation to reduce system carbon emissions. The total installed capacity of energy storage is higher for conventional demand response than for low-carbon demand response at 1347.32MW and 911.13 MW, respectively, suggesting that conventional demand response requires an increase in energy storage capacity to promote the absorption

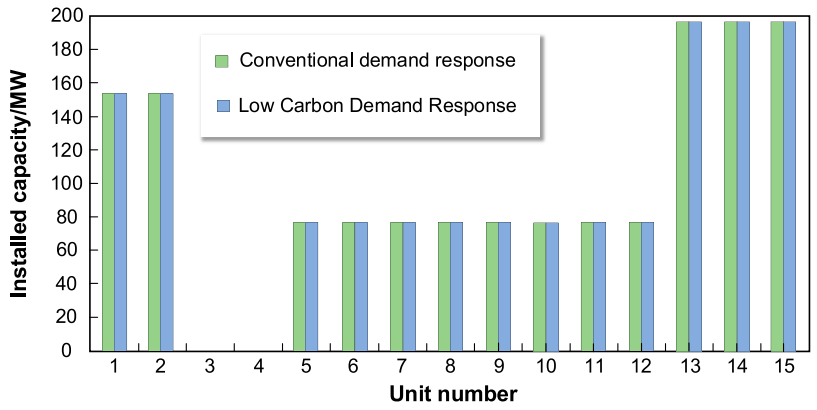

FIGURE 8
Comparison of optimization results of installed capacity of the traditional unit between conventional demand response and low-carbon demand response.

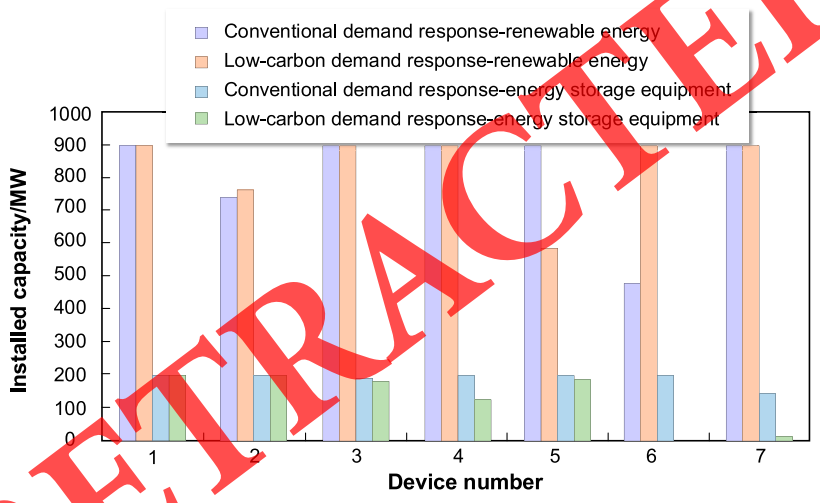

FIGURE 9
Comparison of optimization results of installed capacity of renewable energy and energy storage equipment between conventional demand response and low-carbon demand response.

of new energy, while low-carbon demand response has a stronger capacity for new energy absorption.

4.5 Analysis of low-carbon planning results under different proportions of renewable energy generation

To analyze the impact of different proportions of renewable energy generation on the low-carbon planning method proposed in this paper, calculations were performed for scenarios where the proportion of renewable energy generation is 80% and 90%, respectively. The planning results for these scenarios are shown in Table 2.

From Table 2, it is evident that as the proportion of renewable energy generation increases, the system construction cost increases, but the total carbon emissions and carbon emission costs significantly decrease. This indicates that increasing the amount of renewable energy generation helps reduce both system carbon emissions and carbon emission costs. However, due to the higher investment cost of renewable energy, the overall construction cost of the system increases.

4.6 Analysis of low-carbon planning results under different demand response costs

To analyze the impact of demand response cost on the low-carbon planning method, calculations were performed for scenarios where the demand response cost is 200 yuan/MW and 400 yuan/MW. The planning results for these scenarios are shown in Table 3. As indicated in Table 3, increasing the demand response cost leads to an increase in both the system construction cost and the system carbon emission cost.

TABLE 2 Comparison of cost and total carbon emissions under different power generation proportions of renewable.

Proportion	System investment costs (billion yuan)	System operation cost (billion yuan)	System comprehensive cost (billion yuan)	Total carbon emission cost of the system (billion yuan)	Total carbon emissions of the system (tCO2)
70	841.235	10.294	851.529	16.185	6279634.733
80	975.188	9.048	984.236	10.671	4399616.141
90	1138.564	7.560	1146.124	7.817	3338000.432

TABLE 3 Comparison of cost and total carbon emissions under different demand response costs.

Cost (yuan·MW-1)	System investment costs (billion yuan)	System operation cost (billion yuan)	System comprehensive cost (billion yuan)	Total carbon emission cost of the system (billion yuan)	Total carbon emissions of the system (tCO2)
200	840.865	10.278	851.143	14.188	5502192.771
300	841.235	10.294	851.529	16.185	6279634.733
400	841.367	10.303	851.67	16.243	6522416.664

4.7 Analysis of sensitivity of the model

The proposed dual-layer low-carbon planning model was analyzed and validated on the improved IEEERTS-24 node system. To further validate the model's robustness, we conducted a sensitivity analysis under various scenarios:

1 .Carbon Pricing: By varying carbon prices, we observed that higher prices enhance the economic attractiveness of renewable energy investments, shifting the balance from traditional fossil fuels to cleaner alternatives.
2. Renewable energy availability: Changes in the availability of renewable resources showed the model's flexibility in adjusting energy storage and traditional unit outputs to maintain system stability. Increased renewable energy availability led to higher storage utilization and reduced traditional unit operation.
3. Demand response costs: Varying demand response costs highlighted their impact on system planning. Lower costs facilitated greater flexibility, reducing reliance on traditional units, while higher costs required increased storage capacity to manage peak loads effectively.

This sensitivity analysis confirms the model's robustness and adaptability, providing valuable insights for real-world implementation under different regulatory and market conditions.

5 Carbon pricing mechanism and policy implication

The effectiveness of the proposed dual-layer low-carbon planning model hinges on the presence of a well-defined carbon pricing mechanism. This mechanism signals the cost of carbon emissions, incentivizing both producers and consumers to reduce their carbon footprints.

5.1 Importance of carbon pricing

Cost reflection: Carbon pricing ensures that the cost of carbon emissions is accurately reflected in the economic activities of power generation and consumption. This internalization of external costs is essential for driving investments toward cleaner energy sources.

Behavioral change: By assigning a cost to carbon emissions, carbon pricing influences the behavior of both energy producers and consumers. It encourages the adoption of energy-efficient technologies and practices, thus supporting the transition to a low-carbon power system.

5.2 Role of policymakers

Establishing carbon trading schemes: Policymakers play a crucial role in setting up carbon trading schemes that create a market for carbon credits. These schemes need to be robust and transparent, ensuring that the price of carbon accurately reflects its environmental impact.

Enhancing existing schemes: For regions with existing carbon trading schemes, policymakers should focus on enhancing these frameworks to improve their effectiveness. This could involve setting stricter emission caps, improving monitoring and reporting standards, and ensuring broader market participation.

5.3 Recommendations for policymakers

Designing effective policies: Policies should be designed to ensure that carbon prices are sufficiently high to drive meaningful reductions in emissions. This involves setting ambitious but achievable targets for carbon reductions and regularly reviewing these targets to ensure they remain aligned with climate goals.

Supporting innovation and transition: Policymakers should provide support for innovation in low-carbon technologies. This could include subsidies for research and development, tax incentives for clean energy investments, and funding for pilot projects that demonstrate the feasibility of new technologies.

Ensuring equity and fairness: Carbon pricing policies should consider the socioeconomic impacts on different stakeholders. Measures such as revenue recycling (returning carbon pricing revenues to the public through rebates or dividends) can help mitigate any regressive effects and ensure public support for carbon pricing.

By establishing and enhancing carbon trading schemes that reflect the true cost of carbon emissions, policymakers can create a conducive environment for the successful implementation of the proposed model. This not only drives the transition to a low-carbon power system but also ensures that the economic incentives are aligned with environmental sustainability goals.

6 Comparison with existing studies

6.1 Comparison with study 1

Our study focuses on the optimization of low-carbon power systems by integrating renewable energy sources, storage, and demand-side management. In contrast, the 2024 study (Liu et al., 2024) designs an electricity data trading method based on price game and blockchain to cover investment costs in low-carbon power systems.

(1) Methodology: While their approach utilizes a data trading framework involving data providers, consumers, and a blockchain-based system to manage transactions, our approach employs a dual-layer planning model to optimize power generation, storage, and demand response.
(2) Innovation: The 2024 study innovates by introducing multidimensional electricity data valuation, game-based pricing optimization, and digital watermarking for data protection. Our innovation lies in the comprehensive integration of carbon emission flows and demand response within a dual-layer optimization framework, ensuring grid stability and efficiency.
(3) Outcome: Their method enables power enterprises to profit from electricity data trading, whereas our model enhances the overall low-carbon performance of the power system by optimizing resource allocation and load management.

6.2 Comparison with study 2

The 2019 study (Li et al., 2019) addresses day-ahead and real-time cooperative energy management for multi-energy systems. It introduces an event-triggered distributed algorithm for asynchronous communication and independent calculation among energy bodies. Our study, on the other hand, targets the planning and optimization of power systems with a specific focus on carbon emission reduction and demand-side response.

(1) Methodology: Their approach leverages a distributed coupled optimization problem for energy management, while our model uses a dual-layer structure to separately handle investment planning and operational adjustments.
(2) Innovation: The 2019 study's key innovation is the event-triggered communication strategy that enhances system reliability and scalability. Our contribution is the application of carbon emission theory to attribute carbon responsibilities to the user side, combined with an effective demand response mechanism to achieve low-carbon objectives.
(3) Outcome: The event-triggered algorithm in the 2019 study reduces communication overhead and enhances privacy, while our model systematically improves the low-carbon footprint of the power system through optimized energy source allocation and load adjustments.

By comparing our work with these studies, we demonstrate that while their innovations in data trading and distributed energy management contribute significantly to the field, our model uniquely integrates carbon emission flows and demand-side responses to optimize low-carbon power systems. This comprehensive approach ensures both environmental sustainability and operational efficiency.

7 Conclusion

This paper develops a dual-layer low-carbon planning model based on carbon emission flow and demand response. This model utilizes carbon emission flow theory to apportion carbon emissions from the generation side to the user side, achieving a reasonable and effective allocation of carbon emission responsibilities on the user side. The investment planning model is used as the upper layer model, incorporating unit clustering linearization technology to enhance the solution efficiency of the upper layer planning model, which simulates the operation of the power system over a full year of 8760 h. The demand response model, using carbon price as the price signal, is employed as the lower layer model. This guides the user side in optimizing load demand adjustments to reduce system carbon emissions and carbon emission costs. The proposed low-carbon planning method was analyzed using a modified IEEE RTS-24 node system.

The case study results demonstrate that the model proposed in this paper can effectively increase the utilization rate of renewable energy and promote its absorption by reasonably adjusting the system load distribution through demand response, without changing the total amount of load demand. This approach leads to savings in investment and operating costs of the power system, significantly reducing both the total carbon emissions and carbon emission costs of the system.

Data availability statement

The original contributions presented in the study are included in the article/Supplementary Material; further inquiries can be directed to the corresponding authors.

Author contributions

WW: conceptualization, data curation, formal analysis, funding acquisition, investigation, resources, software, validation, visualization, writing–original draft, and writing–review and editing. XC: conceptualization, formal analysis, investigation, methodology, project administration, resources, software, supervision, validation, and writing–review and editing. JL: conceptualization, formal analysis, funding acquisition, methodology, software, visualization, and writing–original draft. HZ: conceptualization, data curation, investigation, project administration, and writing–original draft. ML: data curation, methodology, project administration, supervision, and writing–review and editing.

Funding

The author(s) declare that financial support was received for the research, authorship, and/or publication of this article. This research was funded by State Grid Shanxi Electric Power Company Technology Project Research on key technologies of carbon tracking and carbon evaluation for new power system, grant number 520530230005.

Conflict of interest

The authors declare that the research was conducted in the absence of any commercial or financial relationships that could be construed as a potential conflict of interest.

The authors declare that this study received funding from State Grid Shanxi Electric Power Company. The funder had the following involvement in the study: study design.

Publisher's note

References

An, K., Song, K.-B., and Hur, K. (2017). Incorporating charging/discharging strategy of electric vehicles into security-constrained optimal power flow to support high renewable penetration. *Energies* 10, 729. doi:10.3390/en10050729

Asgharian, V., and Abdelaziz, M. (2020). A low-carbon market-based multi-area power system expansion planning model. *Electr. Power Syst. Res.* 187, 106500. doi:10.1016/j.epsr.2020.106500

Chen, Y., Li, P., Ren, W., Shen, X., and Cao, M. (2020). Field data–driven online prediction model for icing load on power transmission lines. *Meas. Control* 53, 126–140. doi:10.1177/0020294019878872

Cheng, Y., Zhang, N., Lu, Z., and Kang, C. (2019). Planning multiple energy systems toward low-carbon society: a decentralized approach. *IEEE Trans. Smart Grid* 10, 4859–4869. doi:10.1109/tsg.2018.2870323

Dimitriadis, C. N., Tsimopoulos, E. G., and Georgiadis, M. C. (2023). Optimal bidding strategy of a gas-fired power plant in interdependent low-carbon electricity and natural gas markets. *Energy (Oxf.)* 277, 127710. doi:10.1016/j.energy.2023.127710

Di Somma, M., Yan, B., Bianco, N., Graditi, G., Luh, P. B., Mongibello, L., et al. (2015). Operation optimization of a distributed energy system considering energy costs and exergy efficiency. *Energy Convers. Manag.* 103, 739–751. doi:10.1016/j.enconman.2015.07.009

Guo, W., Wang, Q., Liu, H., and Desire, W. A. (2023). Multi-energy collaborative optimization of park integrated energy system considering carbon emission and demand response. *Energy Rep.* 9, 3683–3694. doi:10.1016/j.egyr.2023.02.051

Haghighi, R., Yektamoghadam, H., Dehghani, M., and Nikoofard, A. (2021). Generation expansion planning using game theory approach to reduce carbon emission: a case study of Iran. *Comput. Ind. Eng.* 162, 107713. doi:10.1016/j.cie.2021.107713

Huang, Y., Lin, Z., Liu, X., Yang, L., Dan, Y., Zhu, Y., et al. (2021). Bi-level coordinated planning of active distribution network considering demand response resources and severely restricted scenarios. *J. Mod. Power Syst. Clean. Energy* 9, 1088–1100. doi:10.35833/mpce.2020.000335

Kang, C., Zhou, T., Chen, Q., Wang, J., Sun, Y., Xia, Q., et al. (2015). Carbon emission flow from generation to demand: a network-based model. *IEEE Trans. Smart Grid* 6, 2386–2394. doi:10.1109/tsg.2015.2388695

Li, J., He, X., Li, W., Zhang, M., and Wu, J. (2023). Low-carbon optimal learning scheduling of the power system based on carbon capture system and carbon emission flow theory. *Electr. Power Syst. Res.* 218, 109215. doi:10.1016/j.epsr.2023.109215

Li, L., Zhang, S., Cao, X., and Zhang, Y. (2021). Assessing economic and environmental performance of multi-energy sharing communities considering different carbon emission responsibilities under carbon tax policy. *J. Clean. Prod.* 328, 129466. doi:10.1016/j.jclepro.2021.129466

Li, Y., Zhang, H., Liang, X., and Huang, B. (2019). Event-triggered-based distributed cooperative energy management for multienergy systems. *IEEE Trans. Industrial Inf.* 15, 2008–2022. doi:10.1109/TII.2018.2862436

Li, Z., Li, X., Lu, C., Ma, K., and Bao, W. (2024). Carbon emission responsibility accounting in renewable energy-integrated DC traction power systems. *Appl. Energy* 355, 122191. doi:10.1016/j.apenergy.2023.122191

Liang, H., and Ma, J. (2022). Data-driven resource planning for virtual power plant integrating demand response customer selection and storage. *IEEE Trans. Ind. Inf.* 18, 1833–1844. doi:10.1109/tii.2021.3068402

Liu, Z., Huang, B., Li, Y., Sun, Q., Pedersen, T., and Gao, D. (2024). Pricing game and blockchain for electricity data trading in low-carbon smart energy systems. *IEEE Trans. Industrial Inf.* 20, 6446–6456. doi:10.1109/TII.2023.3345450

Mei, Z., Jiang, X., and Wang, K. (2022). "Multi-objective coordinated optimal scheduling of virtual power plants based on demand side response," in Proceedings of the 2022 IEEE Asia-Pacific Conference on Image Processing, Electronics and Computers (IPEC), Dalian, China, 14-16 April 2022 (IEEE).

Palmintier, B. S., and Webster, M. D. (2016). Impact of operational flexibility on electricity generation planning with renewable and carbon targets. *IEEE Trans. Sustain. Energy* 7, 672–684. doi:10.1109/tste.2015.2498640

Romero-Ávila, D., and Omay, T. (2022). Are CO2 emissions stationary after all? New evidence from nonlinear unit root tests. *Environ. Model. Assess.* 27, 621–643. doi:10.1007/s10666-022-09835-4

Salahi, S., Rezaei, N., and Moshtagh, J. (2020). An info-gap risk-averse optimization model for coordination of overcurrent protective relays considering power system uncertainty. *Int. Trans. Electr. Energy Syst.* 30. doi:10.1002/2050-7038.12600

Shen, W., Qiu, J., Meng, K., Chen, X., and Dong, Z. Y. (2020). Low-carbon electricity network transition considering retirement of aging coal generators. *IEEE Trans. Power Syst.* 35, 4193–4205. doi:10.1109/tpwrs.2020.2995753

Wan, T., Tao, Y., Qiu, J., and Lai, S. (2023). Internet data centers participating in electricity network transition considering carbon-oriented demand response. *Appl. Energy* 329, 120305. doi:10.1016/j.apenergy.2022.120305

Zhang, J., Tian, G., Chen, X., Liu, P., and Li, Z. (2023). A chance-constrained programming approach to optimal planning of low-carbon transition of a regional energy system. *Energy (Oxf.)* 278, 127813. doi:10.1016/j.energy.2023.127813

Zhao, B., Bukenberger, J., and Webster, M. (2022). Scenario partitioning methods for two-stage stochastic generation expansion under multi-scale uncertainty. *IEEE Trans. Power Syst.* 37, 2371–2383. doi:10.1109/tpwrs.2021.3121369